Subdividing the surface in both the u and w directions yields a 5×5 defining polygon net given by

$C_{1,1}$ [−15 0 15] $C_{2,1}$ [−10 2.5 15]
$C_{1,2}$ [−15 2.5 10] $C_{2,2}$ [−10 5 10]
$C_{1,3}$ [−15 5 0] $C_{2,3}$ [−10 7.5 0]
$C_{1,4}$ [−15 2.5 −10] $C_{2,4}$ [−10 5 −10]
$C_{1,5}$ [−15 0 −15] $C_{2,5}$ [−10 2.5 −15]

$C_{3,1}$ [0 5 15]	$C_{4,1}$ [10 2.5 15]	$C_{5,1}$ [15 0 15]
$C_{3,2}$ [0 7.5 10]	$C_{4,2}$ [10 5 10]	$C_{5,2}$ [15 2.5 10]
$C_{3,3}$ [0 10 0]	$C_{4,3}$ [10 7.5 0]	$C_{5,3}$ [15 5 0]
$C_{3,4}$ [0 7.5 −10]	$C_{4,4}$ [10 5 −10]	$C_{5,4}$ [15 2.5 −10]
$C_{3,5}$ [0 5 −15]	$C_{4,5}$ [10 2.5 −15]	$C_{5,5}$ [15 0 −15]

Note that this net is derivable from either of the two above using Eqs. (5–119) and (5–120).

The original surface and all three of the subdivided surface nets are shown in Fig. 6–51. Each of the surfaces is identical to the original surface.

Clearly, as the surface is further subdivided the defining polygon net converges to the surface.

6–15 GAUSSIAN CURVATURE AND SURFACE FAIRNESS

Of fundamental concern in computer aided design is development of appropriate techniques for determining and/or visualizing the fairness or smoothness of surfaces. It is well known that the bicubic surfaces (Coons, Bézier or B-spline) commonly used, although C^2 continuous everywhere, can exhibit unfair bumps, flat spots or undulations. Currently the best mathematical techniques for determining surface fairness use Eulerian (orthogonal) nets of minimum and maximum curvature (see Refs. 6–28 and 6–29) and of Gaussian curvature (see Refs. 6–28 to 6–32, and Sec. 6–8).

Recalling the discussion of Sec. 6–8, two combinations of the principal curvatures, called the average and the Gaussian (total) curvatures, characterize the local shape of the surface. The average curvature is

$$\kappa_a = \frac{\kappa_{\min} + \kappa_{\max}}{2} \qquad (6-45)$$

The Gaussian curvature is

$$\kappa_g = \kappa_{\min} \cdot \kappa_{\max} \qquad (6-46)$$

where $\kappa_{\min}$ and $\kappa_{\max}$ are the principal curvatures. The Gaussian curvature at a point on the surface indicates whether the surface is locally elliptic, hyperbolic or parabolic (Gaussian curvature positive, negative or zero).

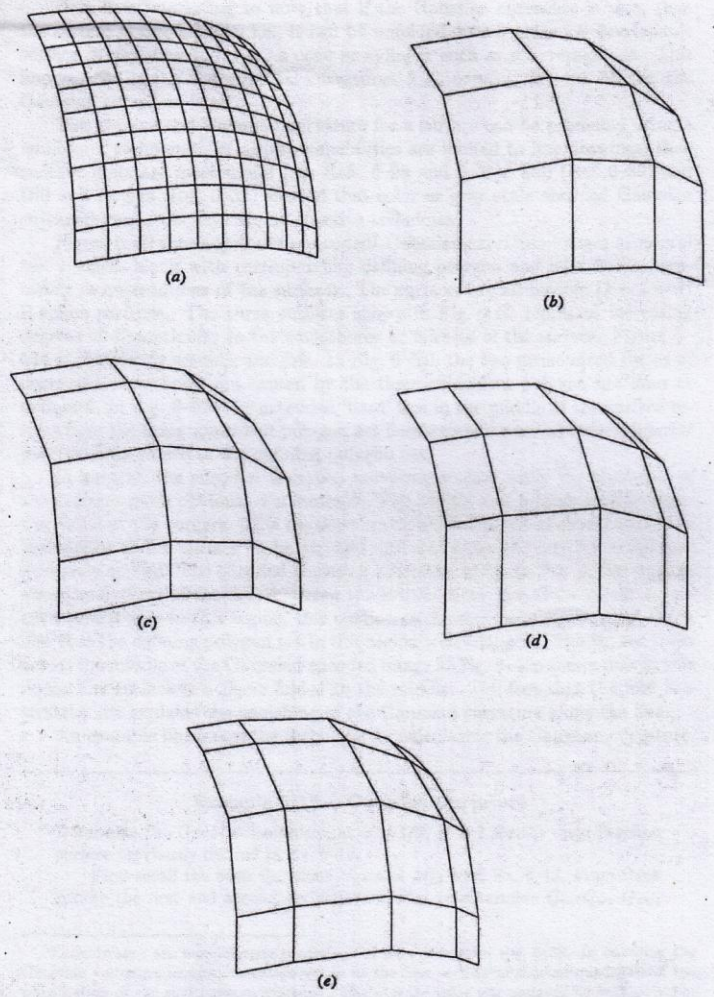

Figure 6–51 B-spline surface subdivision. (a) Surface; (b) original defining polygon net; (c) net subdivided in w; (d) net subdivided in u; (e) net subdivided in both u and w.

Here it is interesting to note that if the Gaussian curvature is zero, then the surface is developable; i.e., it can be unfolded onto a plane. A developable surface is singly curved, e.g., a cone or cylinder such as a beverage can. This implies that one of the principal curvatures, $\kappa_{\min}$ or $\kappa_{\max}$, is zero. Hence, the Gaussian curvature is zero.

The average and Gaussian curvature for a surface can be presented using a number of techniques. If display capabilities are limited to line drawings, then contour plots are most useful (see Refs. 6–28 and 6–29). Dill (Ref. 6–30) and Dill and Rogers (Ref. 6–32) showed that color or gray scale encoded Gaussian curvature raster displays are an effective technique.

Figure 6–52 shows gray scale encoded† Gaussian curvature images of several test surfaces along with corresponding defining polygon and wire frame parametric representations of the surfaces. The surfaces are all bicubic ($k = l = 4$) B-spline surfaces. The three surfaces shown in Fig. 6–52 represent increasing degrees of discontinuity in the smoothness or fairness of the surface. Figure 6–52a is completely smooth and fair. In Fig. 6–52b the two pronounced ridges of decreased smoothness are caused by the three coincident polygon net lines at each end. In Fig. 6–52c the extended 'hard' line in the middle of the surface results from the three coincident polygon net lines extending across several interior polygon lines shown in the defining polygon net.

In general, the encoded Gaussian curvature images make the character of the surfaces more obvious. For example, Figs. 6–52a and b show a large negative value at the corners. This negative curvature is a result of constraining the boundaries of the surface to be straight and flat while the interior is full and positively curved. The encoded Gaussian curvature image in Fig. 6–52b emphasizes the flatness of the area between the ridges. Note that since the Gaussian curvature is zero in this region, this portion of the surface is developable. Note also that the defining polygon net in this region is developable. Finally, the band across the middle of the Gaussian encoded image in Fig. 6–52c shows that in this region the surface is a plane folded in the middle. The fact that the fold is a straight line explains the vanishing of the Gaussian curvature along the line.

An example illustrates the technique for calculating the Gaussian curvature.

Example 6–17 Gaussian Curvature

Determine the Gaussian curvature at $u = 1/2$, $w = 1$ for the open B-spline surface previously defined in Ex. 6–15.

First recall the basis functions $N_{i,4}$ and $M_{j,l}$ from Ex. 6–15. From these results the first and second derivatives needed to determine Q_u, Q_w, Q_{uw},

---

†These images are monochrome renderings of color images in Ref. 6–33. In encoding the Gaussian curvature images, curvature values at the four vertices of a dense quadrilateral approximation of the surface were averaged. The average value was assigned to each polygon. The curvature range was divided into a number of equal intervals (except at the ends) corresponding to the available intensity range. A legend giving this range is shown to the right of the image. The aliasing (staircase-like boundaries between different intensities) is due to the limited number of available intensities and *not* to the polygonal approximation.

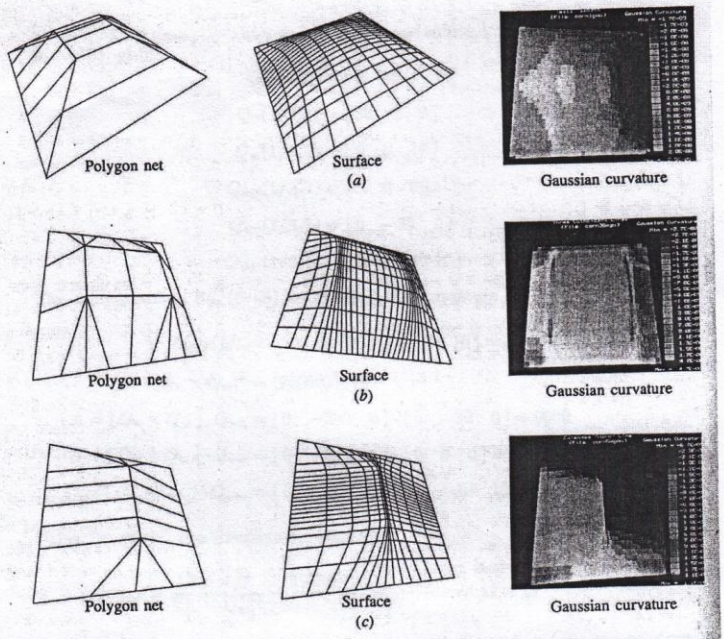

Figure 6–52 Gaussian curvature. (a) Smooth surface; (b) short 'hard' line; (c) longer 'hard' line. (Courtesy J. C. Dill and D. F. Rogers.)

Q_{uu} and Q_{ww}, and subsequently the Gaussian curvature, can be calculated. Specifically,

$$
\begin{array}{lll}
N_{1,4} = (1-u)^3 & N'_{1,4} = -3(1-u)^2 & N_{1,4} = 6(1-u) \\
N_{2,4} = 3u(1-u)^2 & N'_{2,4} = 3(1-u)(1-3u) & N''_{2,4} = 6(3u-2) \\
N_{3,4} = 3u^2(1-u) & N'_{3,4} = 3u(2-3u) & N''_{3,4} = 6(1-3u) \\
N_{4,4} = u^3 & N'_{4,4} = 3u^2 & N''_{4,4} = 6u
\end{array}
$$

and

$$
\begin{array}{lll}
M_{1,3} = 0 & M'_{1,3} = 0 & M''_{1,3} = 0 \\
M_{2,3} = \dfrac{(2-w)^2}{2} & M'_{2,3} = w-2 & M''_{2,3} = 1 \\
M_{3,3} = \dfrac{(2-w)(3w-2)}{2} & M'_{3,3} = 4-3w & M''_{3,3} = -3 \\
M_{4,3} = (w-1)^2 & M'_{4,3} = 2(w-1) & M''_{4,3} = 2
\end{array}
$$

Evaluating the derivatives at $u = 1/2, w = 1$, and substituting into Eqs. (6–71) to (6–75), yields

$$Q(1/2,1) = [\,0 \quad 35/4 \quad 0\,]$$

$$Q_u(1/2,1) = [\,30 \quad 0 \quad 0\,]$$

$$Q_w(1/2,1) = [\,0 \quad 0 \quad 10\,]$$

$$Q_{uw}(1/2,1) = [\,0 \quad 0 \quad 0\,]$$

$$Q_{uu}(1/2,1) = [\,0 \quad -30 \quad 0\,]$$

$$Q_{ww}(1/2,1) = [\,0 \quad -10 \quad 10\,]$$

The components of Eq. (6–48) for the Gaussian curvature are

$$Q_u \times Q_w = [\,30 \quad 0 \quad 0\,] \times [\,0 \quad 0 \quad 10\,] = [\,0 \quad -300 \quad 0\,]$$

$$|Q_u \times Q_w|^4 = (90000)^4$$

$$A = [\,Q_u \times Q_w\,] \cdot Q_{uu} = [\,0 \quad -300 \quad 0\,] \cdot [\,0 \quad -30 \quad 0\,] = 9000$$

$$B = [\,Q_u \times Q_w\,] \cdot Q_{uw} = [\,0 \quad -300 \quad 0\,] \cdot [\,0 \quad 0 \quad 0\,] = 0$$

$$C = [\,Q_u \times Q_w\,] \cdot Q_{ww} = [\,0 \quad -300 \quad 0\,] \cdot [\,0 \quad -10 \quad 10\,] = 3000$$

Using Eq. (6–48) the Gaussian curvature is

$$\kappa_g = \frac{AC - B}{|Q_u \times Q_w|^4} = \frac{(9000)(3000) - (0)}{(90000)^4} = 4.12 \times 10^{-13}$$

Since $\kappa_g > 0$, the surface is locally elliptical.

6–16 RATIONAL B-SPLINE SURFACES

As with rational curves, rational forms of the quadric surfaces, of Coons bicubic surfaces and of Bézier surfaces are possible. However, both because of space limitations and because they represent a generalization of all these forms, only rational B-spline surfaces are considered.

A Cartesian product rational B-spline surface in four-dimensional homogeneous coordinate space is given by

$$Q(u,w) = \sum_{i=1}^{n+1} \sum_{j=1}^{m+1} B_{i,j}^h N_{i,k}(u) M_{j,l}(w) \qquad (6-85)$$

where the $B_{i,j}^h$'s are the 4D homogeneous defining polygon vertices and $N_{i,k}(u)$ and $M_{j,l}(w)$ are the nonrational B-spline basis functions previously given in Eq. (5–84).

Projecting back into three-dimensional space by dividing through by the homogeneous coordinate gives the rational B-spline surface

$$Q(u,w) = \frac{\sum_{i=1}^{n+1}\sum_{j=1}^{m+1} h_{i,j} B_{i,j} N_{i,k}(u) M_{j,l}(w)}{\sum_{i=1}^{n+1}\sum_{j=1}^{m+1} h_{i,j} N_{i,k}(u) M_{j,l}(w)} = \sum_{i=1}^{n+1}\sum_{j=1}^{m+1} B_{i,j} S_{i,j}(u,w) \qquad (6-86)$$

where the $B_{i,j}^h$'s are the 3D defining polygon net points and the $S_{i,j}(u,w)$ are the bivariant rational B-spline surface basis functions

$$S_{i,j}(u,w) = \frac{h_{i,j} N_{i,k}(u) M_{j,l}(w)}{\sum_{i1=1}^{n+1}\sum_{j1=1}^{m+1} h_{i1,j1} N_{i1,k}(u) M_{j1,l}(w)} \qquad (6-87)$$

It is convenient to assume $h_{i,j} \geq 0$ for all i, j.

Here, it is important to note that $S_{i,j}(u,w)$ is *not* the product of $R_{i,k}(w)$ and $R_{j,l}(w)$ (see Eq. 5–123). However, the $S_{i,j}(u,w)$ have similar shapes and analytic properties to the product function $N_{i,k}(u)M_{j,l}(w)$. Hence, rational B-spline surfaces have similar analytic and geometric properties to their nonrational counterparts. Specifically,

The sum of the rational surface basis functions for any u, w values is

$$\sum_{i=1}^{n+1}\sum_{j=1}^{m+1} S_{i,j}(u,w) \equiv 1 \qquad (6-88)$$

Each rational surface basis function is positive or zero for all parameter values u, w, i.e., $S_{i,j} \geq 0$.

Except for $k = 1$ or $l = 1$, each rational surface basis function has precisely one maximum.

The maximum order of a rational B-spline surface in each parametric direction is equal to the number of defining polygon vertices in that direction.

A rational B-spline surface of order k, l (degree $k-1$, $l-1$) is C^{k-2}, C^{l-2} continuous everywhere.

A rational B-spline surface is invariant with respect to a *projective* transformation; i.e., any *projective* transformation can be applied to the surface by applying it to the defining polygon net. Note this is a stronger condition than that for a nonrational B-spline surface.

The surface lies within the convex hull of the defining polygon net formed by taking the union of all convex hulls of k, l neighboring polygon net vertices.

The variation diminishing property is not known for rational B-spline surfaces.

The influence of a single polygon net vertex is limited to $\pm k/2$, $\pm l/2$ spans in each parametric direction.

If triangulated, the defining polygon net forms a planar approximation to the surface.

If the number of defining polygon net vertices is equal to the order in each parametric direction and there are no duplicate interior knot values, the rational B-spline surface is a rational Bézier surface.

From Eqs. (6–86) and (6–87) it is clear that when all $h_{i,j} = 1$, $S_{i,j}(u,w) = N_{i,k}(u)M_{j,l}(w)$. Thus, rational B-spline surface basis functions and surfaces reduce to their nonrational counterparts. Consequently, rational B-spline surfaces represent a proper generalization of nonrational B-spline surfaces and of rational and nonrational Bézier surfaces.

Again, as is the case for rational B-spline curves, algorithms for degree raising, subdivision (see Sec. 6–14) and surface fitting (see Sec. 6–13) of nonrational B-spline surfaces are applicable by simply applying them to the 4D defining polygon net vertices.

Open uniform, periodic uniform and nonuniform knot vectors can be used to generate rational B-spline basis functions and rational B-spline surfaces. Knot vector types can be mixed. For example, an open uniform knot vector can be used in the u parametric direction and a nonuniform knot vector in the w direction. Here we initially concentrate on open uniform knot vectors.

Figure 6–53 shows a bicubic ($k = l = 4$) rational B-spline surface and its defining polygon net for $h_{1,3} = h_{2,3} = 0, 1, 5$. Figure 6–53c, with $h_{1,3} = h_{2,3} = 1$, is identical to the nonrational B-spline surface. The effects of varying the homogeneous coordinate values can be seen by comparing Fig. 6–53c to Figs. 6–53b and d. The effects are analogous to, but not as striking as, those for rational B-spline curves (see Sec. 5–13). Here the effects are reduced by the fact that $S_{i,j}(u,w)$ is a bivariate blending function.

Figures 6–54a and b illustrate the effect obtained by setting all interior $h_{i,j}$'s = 0 and 500, respectively; i.e., $h_{2,2} = h_{2,3} = h_{3,2} = h_{3,3} = h_{4,2} = h_{4,3} = 0, 500$. All other $h_{i,j}$'s = 1. The defining polygon net is shown in Fig. 6–53a. Setting all the interior $h_{i,j}$'s = 0 effectively ignores the interior defining polygon net vertices. Only the edge vertices are interpolated. In contrast, setting all the interior $h_{i,j}$'s = 500 reduces the influence of the edge vertices to a minimum. Note that changing the $h_{i,j}$'s affects the parameterization of the surface. This effect is illustrated by the clustering of the parametric lines near the edges of the surface when the interior $h_{i,j}$'s = 0 (see Fig. 6–54a) and in the interior of the surface when the interior $h_{i,j}$'s = 500 (see Fig. 6–54b).

The effects of multiple vertices or net lines are analogous to those for nonrational B-spline surfaces (see Sec. 6–12) and of rational B-spline curves (see Sec. 5–13). The results of moving a single vertex on the surface are also analogous.

One of the strong attractions of rational B-spline surfaces is their ability to represent quadric surfaces *and* to blend them smoothly into higher degree

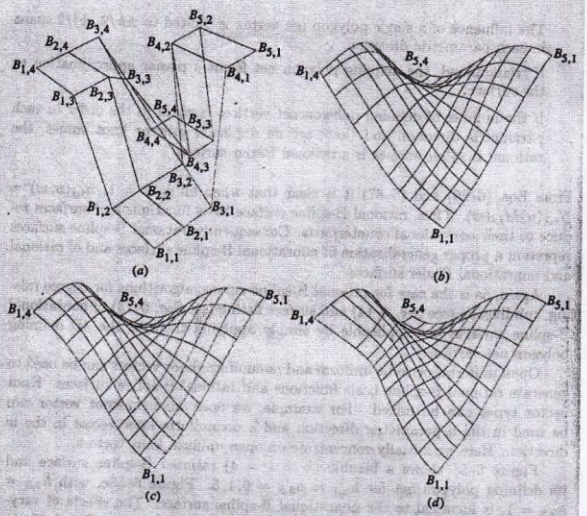

Figure 6–53 Rational B-spline surfaces with $n+1=5$, $m+1=4$, $k=l=4$. (a) Defining polygonal net; (b) $h_{1,3}=h_{2,3}=0$; (c) $h_{1,3}=h_{2,3}=1$; (d) $h_{1,3}=h_{2,3}=5$.

sculptured surfaces. As a simple example of a quadric surface consider a general cylinder formed by sweeping a curve. It is clear that the surface must be second order, i.e., a straight line, in the sweep direction. Consequently, with the surface swept out in the u parametric direction, the surface representation is (see Ref. 6–33)

$$Q(u,w)=\sum_{i=1}^{2}\sum_{j=1}^{m+1}B_{i,j}S_{i,j}(u,w) \qquad (6-89)$$

where $S_{i,j}(u,w)$ is of the order of the curve in the w parametric direction and of order 2 in the u parametric direction. Further, the defining polygon net vertices in the u direction are $B_{1,j}=B_j$ and $B_{2,j}=B_j+sD$, where D gives the direction and distance to be swept. s is a parameter in the range $0\le s\le 1$. The B_j's are the defining polygon vertices for the swept curve. The homogeneous coordinates are maintained constant in the sweep direction; i.e., $h_{1,j}=h_{2,j}=h_j$ where h_j is

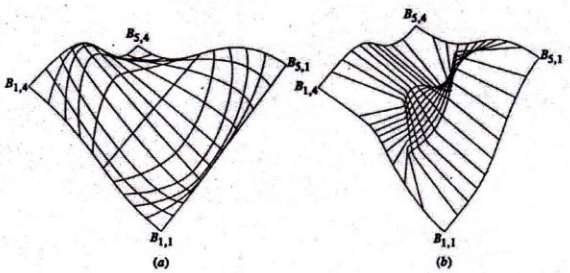

Figure 6–54 Rational B-spline surfaces with $n+1=5$, $m+1=4$, $k=l=4$. (a) All interior $h_{i,j}$'s $= 0$; (b) all interior $h_{i,j}$'s $= 500$.

the homogeneous coordinate for the swept curve. Figure 6–55a shows an elliptic cylinder generated using the elliptic curve given in Fig. 5–67b. The swept curve is shown offset at each end.

Rational B-spline surfaces are also used to generate ruled surfaces. The elliptic cylinder shown in Fig. 6–55 is of course a ruled surface. The conditions required to generate a more general ruled surface, using rational B-splines, require that both curves be of the same order (degree), have the same knot vector and have the same number of defining polygon vertices. If the curves are not of the same order (degree) the degree of the lower order curve is raised (see Sec. 5–8 and Ex. 6–18). The required knot vector is the union of the knot vectors of the two curves. Any multiplicity of knot values for either curve is included in the

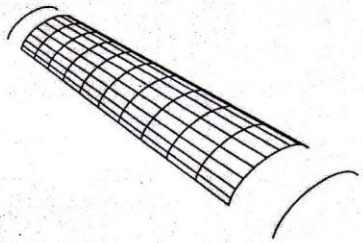

Figure 6–55 Rational B-spline elliptic cylinder generated by sweeping the rational elliptic curve of Fig. 5–67b.

final knot vector. Knot insertion (see Sec. 5–12) is used to insure that both knot vectors are identical. Degree raising and knot insertion insure that the number of defining polygon vertices is identical for both curves. The resulting rational B-spline ruled surface is described by Eq. (6–89) with

$$P_1(w) = Q(0,w) = \sum_{j=1}^{m+1} B_{1,j} R_{j,l}(w) \quad \text{and} \quad P_2(w) = \sum_{j=1}^{m+1} B_{2,j} R_{j,l}(w) = Q(1,w)$$

Figure 6–56 shows an example of a ruled surface blending a quarter circle into a fourth order rational B-spline curve. The curves and their defining polygons are shown offset at each end. An example better illustrates the technique.

Example 6–18 Rational B-spline Ruled Surface

Determine the point at $u = w = 0.5$ on a ruled surface formed by blending a 120° circular arc represented by a third order rational B-spline curve defined by $B_{1,1}[0 \;\; 0 \;\; 0]$, $B_{1,2}[1 \;\; \sqrt{3} \;\; 0]$, $B_{1,3}[2 \;\; 0 \;\; 0]$ and $[H] = [1 \;\; 1/2 \;\; 1]$, with a fourth order rational curve defined by $B_{2,1}[0 \;\; 0 \;\; 10]$, $B_{2,2}[1 \;\; 1 \;\; 10]$, $B_{3,2}[2 \;\; 0 \;\; 10]$, $B_{4,2}[3 \;\; 1 \;\; 10]$ with $[H] = [1 \;\; 3/4 \;\; 5 \;\; 1]$.

First it is necessary to raise the degree of the circular arc. The circular arc is in fact a rational Bézier curve. For the rational case the degree raising technique discussed in Sec. 5–8 is applied to the 4D homogeneous coordinates. The results are:

$$B_1^{h*} = B_1^h$$

$$B_i^{h*} = \alpha_i B_{i-1}^h + (1-\alpha_i) B_i^h \qquad \alpha_i = \frac{i}{n+1} \qquad i = 2, \cdots, n$$

$$B_{n+1}^{h*} = B_n^h$$

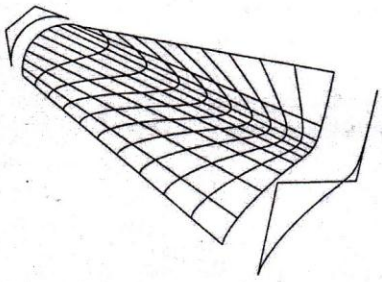

Figure 6–56 Rational B-spline ruled surface.

Projecting back into 3D space yields

$$B_1^* = B_1$$

$$B_i^* = \frac{\alpha_i h_{i-1} B_{i-1} + (1-\alpha_i) h_i B_i}{\alpha_i h_{i-1} + (1-\alpha_i) h_i} \qquad i = 2, \cdots, n$$

$$h_i^* = \alpha_i h_{i-1} + (1-\alpha_i) h_i$$

Using these results to raise the degree of the 120° arc yields

$$h_{1,1}^* = h_{1,1} = 1$$

$$B_{1,1}^* = B_{1,1} = [0 \quad 0 \quad 0]$$

$$h_{1,2}^* = \left(\frac{1}{3}\right)(1) + \left(\frac{2}{3}\right)\left(\frac{1}{2}\right) = \frac{2}{3}$$

$$B_{1,2}^* = \left\{\frac{1}{3}(1)[0 \quad 0 \quad 0] + \frac{2}{3}\left(\frac{1}{2}\right)[1 \quad \sqrt{3} \quad 0]\right\} \Big/ \left(\frac{2}{3}\right) = \left[\frac{1}{2} \quad \frac{\sqrt{3}}{2} \quad 0\right]$$

$$h_{1,3}^* = \left(\frac{2}{3}\right)\left(\frac{1}{2}\right) + \left(\frac{1}{3}\right)(1) = \frac{2}{3}$$

$$B_{1,3}^* = \left\{\left(\frac{2}{3}\right)\left(\frac{1}{2}\right)[1 \quad \sqrt{3} \quad 0] + \frac{1}{3}(1)[2 \quad 0 \quad 0]\right\} \Big/ \left(\frac{2}{3}\right) = \left[\frac{3}{2} \quad \frac{\sqrt{3}}{2} \quad 0\right]$$

$$h_{1,4}^* = h_{1,3} = 1$$

$$B_{1,4}^* = B_{1,3} = [2 \quad 0 \quad 0]$$

Each curve now has four defining polygon vertices. The knot vector for each curve is $[X] = [Y] = [0 \quad 0 \quad 0 \quad 0 \quad 1 \quad 1 \quad 1 \quad 1]$. Hence knot insertion is unnecessary.

For $u = w = 0.5$ Eq. (5–84) yields

$$N_{1,2} = 0.5; \qquad N_{2,2} = 0.5$$

$$M_{1,4} = 0.125; \qquad M_{2,4} = 0.375; \qquad M_{3,4} = 0.375; \qquad M_{4,4} = 0.125$$

Eq. (6–87) then yields

$$S_{1,1} = 0.0396; \qquad S_{1,2} = 0.0792 \qquad S_{1,3} = 0.0792 \qquad S_{1,4} = 0.0396$$

$$S_{2,1} = 0.0396; \qquad S_{2,2} = 0.0891 \qquad S_{2,3} = 0.594 \qquad S_{2,4} = 0.0396$$

The surface point is

$$Q(0.5, 0.5) = [1.634 \quad 0.266 \quad 7.624]$$

Complete results are shown in Fig. 6–56.

Surfaces of revolution can also be represented by rational B-splines. Assuming that

$$P(w) = \sum_{j=1}^{m+1} B_j R_{j,l}(w)$$

with knot vector $[\,Y\,]$ is a rational B-spline curve, and recalling that a full circle is obtained by combining four quarter circles defined by nine polygon vertices (see Sec. 5–13), leads to a rational B-spline surface of revolution defined by (see Ref. 6–33)

$$Q(u,w) = \sum_{i=1}^{9} \sum_{j=1}^{m+1} B_{i,j} S_{i,j}(u,w) \qquad (6-90)$$

where the knot vector $[\,X\,] = [\,0\ \ 0\ \ 0\ \ 1\ \ 1\ \ 2\ \ 2\ \ 3\ \ 3\ \ 4\ \ 4\ \ 4\,]$. Assuming that rotation occurs about the z-axis and that the curve $P(w)$ is defined in the xz plane, the $B_{i,j}$'s are given by $B_{1,j} = B_j$ for fixed j with $1 \leq i \leq 9$. The defining polygon vertices form the corners and midpoints of a square lying in a plane perpendicular to the z-axis with side dimension twice the radius of the circle of revolution. The homogeneous weighting factors are the product of those for the defining rational B-spline curve and those required to define the circle of revolution. Specifically, for fixed j, $h_{1,j} = h_j$, $h_{2,j} = h_j\sqrt{2}/2$, $h_{3,j} = h_j$, $h_{4,j} = h_j\sqrt{2}/2, \cdots, h_{9,j} = h_j$. Figure 6–57 shows the defining polygon net and curve for the rational B-spline curve to be rotated and the circle of revolution. Also shown in Fig. 6–57 is the composite surface defining polygon net and the surface itself.

The common quadric surfaces of revolution, e.g., the torus and the sphere along with their defining polygon nets, are shown in Figs. 6–58 and 6–59. The torus is generated by revolving an offset circle about one of the axes. The sphere is generated by revolving a semicircle composed of two 90° arcs about an axis which is a diameter of the semicircle.

As mentioned above, one of the most powerful characteristics of rational versus nonrational B-spline surfaces is their ability to 'bury' or include quadric surface elements within a general sculptured surface. For example, a cylindrical surface element can be included as a part of a more general surface. Figure 6–60 shows three examples. The central portion of each fourth order surface is a section of a circular cylinder. Figure 6–60a might represent the leading edge of a wing or turbine blade.† Figure 6–60b might represent the cylindrical bow (stem) of a ship. Both surfaces are generated by first defining a third order circular arc (see Sec. 5–13), raising the degree of the arc (see Ex. 6–18), making a ruled surface from the arc and including it between the two fourth order side surface elements. Incidentally, both of the surfaces shown in Figs. 6–60a and b are ruled developable surfaces. Figure 6–60c shows the cylindrical element buried in a more general surface.

The derivatives of a rational B-spline surface are obtained by formal differentiation of Eq. (6–86). The results are

$$Q_u = \frac{\bar{N}}{\bar{D}}\left(\frac{\bar{N}_u}{\bar{N}} - \frac{\bar{D}_u}{\bar{D}}\right) \qquad (6-91a)$$

†NACA airfoil sections use a circular arc to define the leading edge.

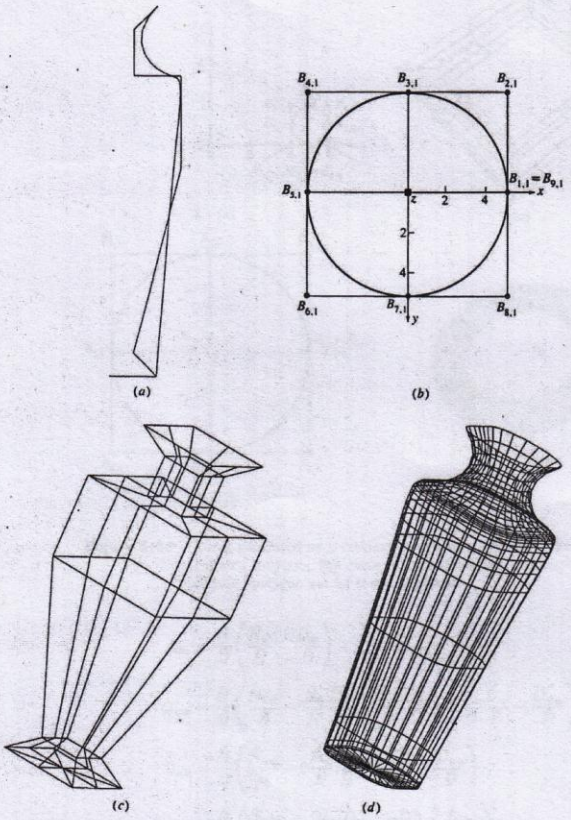

Figure 6–57 Rational B-spline surface of revolution. (a) Generating curve and defining net; (b) circle of revolution; (c) defining surface polygon net; (d) surface of revolution.

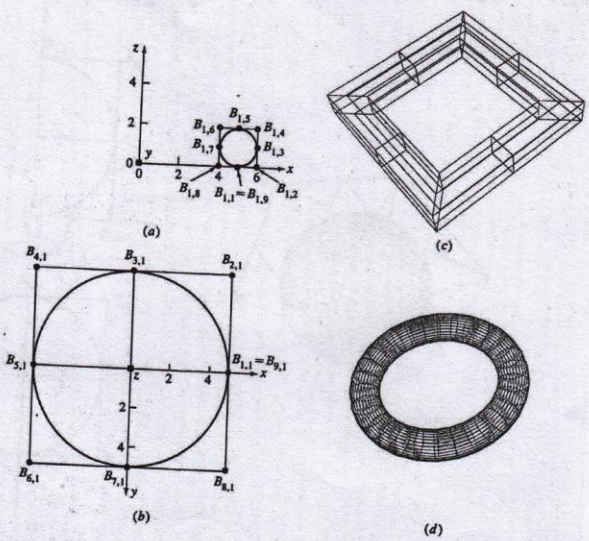

Figure 6–58 Torus generated as a rational B-spline surface. (a) Offset circle and defining polygon; (b) circle of revolution and defining polygon; (c) defining polygon net for torus; (d) torus.

$$Q_w = \frac{\bar{N}}{\bar{D}}\left(\frac{\bar{N}_w}{\bar{N}} - \frac{\bar{D}_w}{\bar{D}}\right) \tag{6-91b}$$

$$Q_{uw} = \frac{\bar{N}}{\bar{D}}\left(\frac{\bar{N}_{uw}}{\bar{N}} - \frac{\bar{N}_u}{\bar{N}}\frac{\bar{D}_w}{\bar{D}} - \frac{\bar{N}_w}{\bar{N}}\frac{\bar{D}_u}{\bar{D}} + 2\frac{\bar{D}_u}{\bar{D}}\frac{\bar{D}_w}{\bar{D}} - \frac{\bar{D}_{uw}}{\bar{D}}\right) \tag{6-91c}$$

$$Q_{uu} = \frac{\bar{N}}{\bar{D}}\left(\frac{\bar{N}_{uu}}{\bar{N}} - 2\frac{\bar{N}_u}{\bar{N}}\frac{\bar{D}_u}{\bar{D}} + 2\frac{\bar{D}_u^2}{\bar{D}^2} - \frac{\bar{D}_{uu}}{\bar{D}}\right) \tag{6-91d}$$

$$Q_{ww} = \frac{\bar{N}}{\bar{D}}\left(\frac{\bar{N}_{ww}}{\bar{N}} - 2\frac{\bar{N}_w}{\bar{N}}\frac{\bar{D}_w}{\bar{D}} + 2\frac{\bar{D}_w^2}{\bar{D}^2} - \frac{\bar{D}_{ww}}{\bar{D}}\right) \tag{6-91e}$$

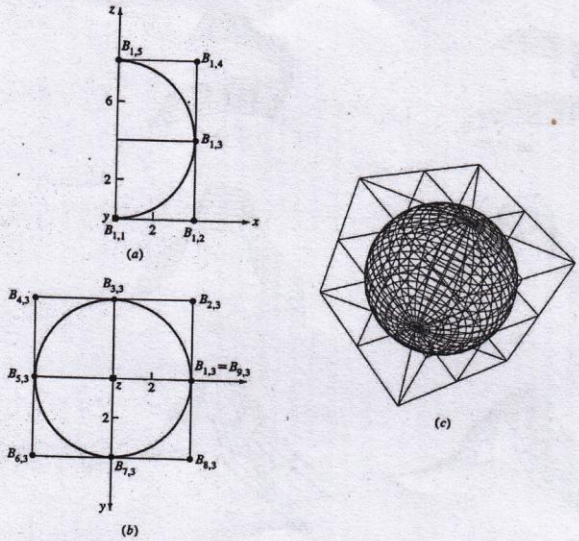

Figure 6–59 Sphere generated as a rational B-spline surface. (a) Offset circle and defining polygon; (b) circle of revolution and defining polygon; (c) defining polygon net and sphere.

where $\bar{N}$ and $\bar{D}$ are the numerator and denominator, respectively, of Eq. (6–86) with derivatives

$$\bar{N}_u = \sum_{i=1}^{n+1} \sum_{j=1}^{m+1} h_{i,j} B_{i,j} N'_{i,k}(u) M_{j,l}(w)$$

$$\bar{N}_w = \sum_{i=1}^{n+1} \sum_{j=1}^{m+1} h_{i,j} B_{i,j} N_{i,k}(u) M'_{j,l}(w)$$

$$\bar{N}_{uw} = \sum_{i=1}^{n+1} \sum_{j=1}^{m+1} h_{i,j} B_{i,j} N'_{i,k}(u) M'_{j,l}(w)$$

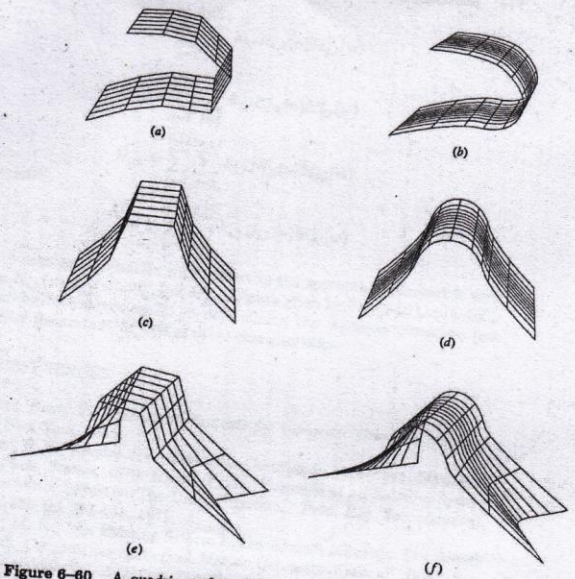

Figure 6–60 A quadric surface element within a more general rational B-spline surface. Airfoil leading edge. (a) Polygon net; (b) surface. Ship stern. (c) Polygon net; (d) surface. A cylinder as part of a more general surface. (e) Polygon net; (f) surface.

$$\tilde{N}_{uu} = \sum_{i=1}^{n+1} \sum_{j=1}^{m+1} h_{i,j} B_{i,j} N''_{i,k}(u) M_{j,l}(w)$$

$$\tilde{N}_{ww} = \sum_{i=1}^{n+1} \sum_{j=1}^{m+1} h_{i,j} B_{i,j} N_{i,k}(u) M''_{j,l}(w)$$

$$\tilde{D}_u = \sum_{i=1}^{n+1} \sum_{j=1}^{m+1} h_{i,j} N'_{i,k}(u) M_{j,l}(w)$$

$$\bar{D}_w = \sum_{i=1}^{n+1}\sum_{j=1}^{m+1} h_{i,j} N_{i,k}(u) M'_{j,l}(w)$$

$$\bar{D}_{uw} = \sum_{i=1}^{n+1}\sum_{j=1}^{m+1} h_{i,j} N'_{i,k}(u) M'_{j,l}(w)$$

$$\bar{D}_{uu} = \sum_{i=1}^{n+1}\sum_{j=1}^{m+1} h_{i,j} N''_{i,k}(u) M_{j,l}(w)$$

$$\bar{D}_{ww} = \sum_{i=1}^{n+1}\sum_{j=1}^{m+1} h_{i,j} N_{i,k}(u) M''_{j,l}(w)$$

The prime denotes a derivative with respect to the appropriate parametric variable. The $N'_{i,k}(u)M'_{j,l}(w)$, $N''_{i,k}(u)$, $M''_{j,l}(w)$'s are given by Eq. (5–97) to (5–100). These derivatives are useful in determining the Gaussian curvature (see Sec. 6–15) of the surface, as well as other characteristics.

6–17 REFERENCES

6–1 Rogers, David F., *Procedural Elements for Computer Graphics*, McGraw-Hill, New York, 1985.

6–2 Bézier, P. E., *Emploi des Machines à Commande Numerique*, Masson et Cie, Paris, France, 1970; Bézier, P. E., "Example of an Existing System in the Motor Industry: The Unisurf System," *Proc. Roy. Soc.* (*London*), Vol. A321, pp. 207–218, 1971.

6–3 Sabin, M. A., "An Existing System in the Aircraft Industry. The British Aircraft Corporation Numerical Master Geometry System," *Proc. Roy. Soc.* (*London*), Vol. A321, pp. 197–205, 1971.

6–4 Peters, G. J., "Interactive Computer Graphics Application of the Bicubic Parametric Surface to Engineering Design Problems," McDonnell Douglas Automation Company, St. Louis, Missouri, presented at SIAM 1973 National Meeting, Hampton, Va., 18–21 June 1973.

6–5 Rogers, D. F., and Satterfield, S. G., "Dynamic B-Spline Surfaces," *Proc. of the Fourth International Conference on Computer Applications in the Automation of Shipyard Operation and Ship Design* (ICCAS 82), 7–10 June 1982, Annapolis, Maryland, pp. 189–196, North Holland, 1982.

6–6 Rogers, D. F., and Satterfield, S. G., "B-Spline Surfaces for Ship Hull Design," *Comp. Graph.*, Vol. 14, pp. 211–217, 1980, (SIGGRAPH 80).

6–7 Rogers, D. F., Rodriguez, F., and Satterfield, S. G., "Computer Aided Ship Design and the Numerically Controlled Production of Towing Tank Models," *Proc. of 16th Des. Auto. Conf.*, San Diego, California, 24–27 June 1979.

6–8 Cohen, E., "Some Mathematical Tools for a Modeler's Workbench," *IEEE Comp. Graph. & Appl.*, Vol. 3, pp. 63–66, October 1983.